

MINIMAL TWIN SURFACES

HAO CHEN

ABSTRACT. We report some minimal surfaces that can be seen as copies of a triply periodic minimal surface related by reflections in parallel planes. We call them *minimal twin surfaces* for the resemblance with crystal twinning. Twinning of Schwarz' Diamond and Gyroid surfaces have been observed in experiment by material scientists. In this paper, we investigate twinings of rPD surfaces, a family of rhombohedral deformations of Schwarz' Primitive (P) and Diamond (D) surfaces, and twinings of the Gyroid (G) surface. Small examples of rPD twins have been constructed in Fijomori and Weber (2009), where we observe non-examples near the helicoid limit. Examples of rPD twins near the catenoid limit follow from Traizet (2008). Large examples of rPD and G twins are numerically constructed in Surface Evolver. A structural study of the G twins leads to new description of the G surface in the framework of Traizet.

1. INTRODUCTION

In material science, a *crystal twinning* refers to a symmetric coexistence of two or more crystals related by Euclidean motions. The simplest situation, namely the *reflection twin*, consists of two crystals related by a reflection in the boundary plane.

Triply periodic minimal surfaces (TPMS) are minimal surfaces with the symmetries of crystals. They are used to model lyotropic liquid crystals and many other structures in nature. Recently, [Han et al., 2011] synthesized mesoporous crystal spheres with polyhedral hollows. A crystallographic study shows a structure of Schwarz' D (diamond) surface. Most interestingly, twin structures are observed at the boundaries of the domains; see Figure 1. In the language of crystallography, the twin boundaries are $\{111\}$ planes. We also notice Figure 7.1(b) in [Hyde et al., 1996], which seems like another evidence, but did not catch the attention. [Han et al., 2011] also observed twinning of Schoen's G (gyroid) surface with $\{211\}$ twin boundaries, which was discovered earlier in [Vignolini et al., 2012].

However, it is mathematically premature to call the observed structures "minimal twin surfaces". Despite the common belief and various convincing explanations, the energetic base of mesophased systems forming periodic minimal surfaces is not well understood. Hence we could not say for sure that the observed surface is minimal. Moreover, it is *a priori* not known that a minimal surface with the observed twin structure exists. And even worse, there is not yet a well-defined notion of "minimal twin surface" in mathematics. Because of the analyticity of minimal surfaces, the definition of twinning in physics does not apply to TPMS.

In this note, we report some minimal surfaces that deserve the name "minimal twin surfaces". They are similar to polysynthetic crystal twinings, treating a TPMS as crystal. More specifically, given a TPMS P , the (polysynthetic) *twinning of P* , or simply *P twin*, is a minimal surface Φ with parallel symmetry planes, usually assumed to be horizontal (orthogonal to the z -axis), such that the part of Φ between two nearest symmetry planes is "similar" to P .

The word "similar" is open to interpretations for general situations. The minimum requirement is that the twin surface Φ inherit some symmetries from the original surface P ; see Section 2. Horizontal translational symmetries derived from P are at least included; hence Φ is a TPMS. A main goal of this note is to twin rPD surfaces, a 1-parameter family of rhombohedral deformations of Schwarz' D and P (primitive) surfaces. Then, in addition to the translational symmetries, we require that the rPD twins to have vertical symmetry planes (parallel to the z axis) reflections in

2010 *Mathematics Subject Classification*. Primary 53A10, 49Q05.

Key words and phrases. Triply periodic minimal surfaces, Twin lattice, Surface Evolver.

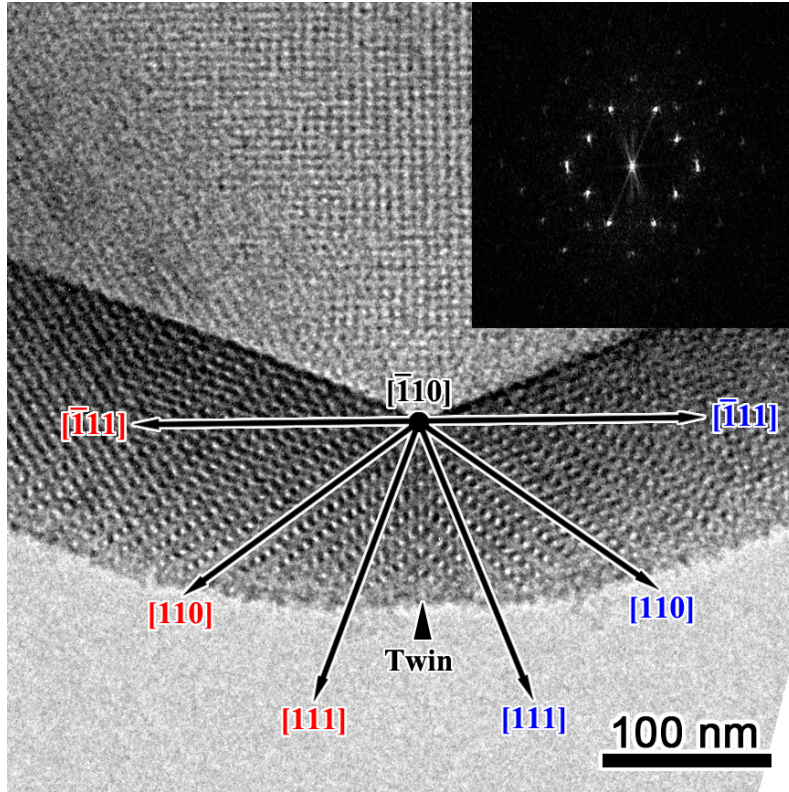


FIGURE 1. Twin structure in minimal D surface observed in experiment. Reuse with permission from [Han et al., 2011]. Copyright ©2011 American Chemical Society.

which form a $(3, 3, 3)$ -triangle group. This is the symmetry of (111) lattice planes of rhombohedral lattice.

Apart from the symmetries, the “similarity” is interpreted case by case for the moment. In this manuscript, it is either encoded in the Weierstrass representation (for rPD-twins, see Definition 3), or operationally defined by Surface Evolver program (see Sections 3.5 and 4.1).

Assume that the original TPMS P is of genus 3, which is the case for rPD surfaces and the G surface. We then parametrize the twinings of P by an integer $n > 0$ such that the twin of parameter n , as a TPMS, is of genus $2n + 1$. For larger n , the part between two nearest symmetry planes correspond to a larger piece of P . In addition, rPD twins are parameterized by a real number $t > 0$, which indicates the distance of the original surface from the catenoid limit. The parameters will be put in subscript, e.g. $\Phi_{t,n}$.

Our main observation is the following:

Observation 1. *rPD twin and G twin surfaces exist for a large set of parameters.*

Examples of rPD twins has been described by [Fujimori and Weber, 2009], but the period problem is only solved for small n . Following their work, we observe that, even when $n = 3$, an rPD twin with sufficiently large t does not exist. On the other hand, for any n , examples with sufficiently small t (near the catenoid limit) follows from [Traizet, 2008].

For large n and t , exact calculation is very challenging. We then use Brakke’s Surface Evolver [Brakke, 1992], an efficient gradient descender, for construction. We obtain a minimal surface if we manage to reduce the integral of squared mean curvature down to practically 0. In this way, we are able to numerically construct D twin for n as large as 299. In particular, it is now reasonable to believe that the D twin observed in experiment is indeed a minimal twin surface. If t and n are too large, our calculation is inconclusive.

Examples of G twins are numerically constructed in Surface Evolver. A structural analysis of G twins leads to a new way to understand the G surface in the framework of [Traizet, 2008]. This leads us to speculate mG, a 3-dimensional family of monoclinic deformations of the G surface. In particular, the alleged mG family seems to contain the tD family.

This note is organized as follows. In Section 2 we discuss the symmetries of TPMS twinning in analogy with crystal twinning. Despite the lack of a general definition, these symmetries are the minimum requirement for a surface to be called “minimal twin surface”. In Section 3, we introduce the rPD surfaces, define their twins by Weierstrass representation, and present rigorous examples with small n (Section 3.3) or small t (Section 3.4) and numerical examples in Surface Evolver (Section 3.5). The G twins are numerically constructed and described in Section 4, after which we speculate and discuss the mG family.

ACKNOWLEDGEMENT

This manuscript, while self-contained, presents mathematical context and technical details as a complement and extension to another paper in preparation on material science. I would like to thank my collaborators in that project, especially Chenyu Jin, Lu Han and Nobuhisa Fujita, for their help on this note. I’m very grateful to Karsten Groß-Brauckmann for valuable suggestions, to Matthias Weber for his comments and Mathematica programs, and to Han Yu and Martin Traizet for helpful discussions. Most of the work was done while the author is visiting St Andrews University.

2. CRYSTAL TWINNING AND TPMS TWINNING

The notion of “TPMS twinning” is not mathematically well defined, and we have no intention to give a definition that works in general situations; this could be an impossible task. The term “minimal twin surface” refers to a minimal surface that is similar to a twin crystal, treating TPMS as the crystal. Here, the word “similar” is open for interpretations, but some rules should be followed. In this section, we summarise the symmetries that we expect for a minimal twin surface, in analogy with crystal twinning.

In physics, a crystal is modeled by a *Bravais lattice*, which can be defined as a discrete point set $\Lambda \subset \mathbb{R}^3$ invariant under three linearly independent translations. A *lattice plane* of Λ is a plane H such that $H \cap \Lambda$ is non-empty and invariant under two linearly independent translations (hence a 2-dimensional lattice). We say that H is *trivial* if Λ is symmetric about H . The *reflection twin* of Λ about a non-trivial lattice plane H consists of lattice points of Λ on one side of H , and their reflective images on the other side. We call H the *twin boundary*. Bravais lattice is however an idealized model. In reality, twinning a lattice will introduce inhomogeneity to the energy, hence atoms near the twin boundary will be slightly pulled away from their original positions.

In mathematics, a lattice may be seen as a discrete group acting on \mathbb{R}^3 by translations. A *triply periodic minimal surface* (TPMS) $P \subset \mathbb{R}^3$ is an *oriented* minimal surface invariant under the action of a lattice Λ . The quotient P/Λ is called the *translational unit*¹. A plane H is a *lattice plane* of P if $H \cap P$ is invariant under the action of a 2-dimensional lattice, and H is *trivial* if P is invariant under the reflection in H . Planes parallel to a lattice plane are lattice planes with the same translational symmetries.

Remark. In this note, the planes of interest are usually placed parallel or orthogonal to the z -axis. But from time to time, we will use Miller indices to denote the directions of lattice planes and directions. Here is a quick reference for readers who are not familiar with the notation: For a lattice spanned by vectors a_1, a_2, a_3 , let h, k and l be three integers. Then $[hkl]$ denotes the direction of the vector $ha_1 + ka_2 + la_3$; (hkl) denotes the lattice plane passing through $a_1/h, a_2/k$ and a_3/l or its parallel planes; $\langle hkl \rangle$ denotes directions that are equivalent to $[hkl]$ by symmetry; and $\{hkl\}$ denotes lattice planes that are equivalent to (hkl) by symmetry. Negative numbers in Miller index will be replaced by a number with bar, such as $\bar{1}$ for -1 .

¹The crystallographic term is “primitive unit cell”.

There are several ways to extract a concrete Bravais lattice from a TPMS. For the TPMS that we are interested in (rPD and G surfaces), we find it convenient to use flat points as lattice points. Let Λ be the Bravais lattice of flat points. It is possible that a TPMS lattice plane H contains no point from Λ , hence not a Bravais lattice plane. We use an *offset* to describe the position of H with respect to Λ : The offset of H varies linearly between in $[0, 1)$; offset 0 means that H contains flat points, and offset 0.5 indicates that H is in the middle of two lattice planes of Λ . Moreover, the *separation* of two TPMS lattice planes refers to the number of Bravais lattice planes between them.

Like Bravais lattices, TPMS often admit extra symmetries other than the translations. The *symmetry group* or *space group* of a TPMS P , denoted by $\text{Sym}(P)$, is the group of Euclidean symmetries of P . For a lattice plane H of P , $\text{Sym}(H)$ denotes the group of symmetries of $H \cap P$ induced by the symmetries in $\text{Sym}(P)$. Parallel lattice planes have the same symmetry.

We could imitate the definition of crystal twinning in physics: take the part of P on one side of H and reflect it to the other side. However, as long as H is non-trivial, the surface obtained is usually not smooth on the twin boundary, hence definitely not a minimal surface. Local minimization of the area functional will inevitably cause a perturbation near the twin boundary. In this sense, TPMS seems more realistic than Bravais lattices. However, it is very difficult to come up with a formal definition for general situation.

As in the case of crystal twinning, we expect the reflection twin of P about H to be invariant under the action of $\text{Sym}(H)$. In particular, $\text{Sym}(H)$ contains a 2-dimensional lattice, hence

Definition 1. Let $P \subset \mathbb{R}^3$ be a triply periodic minimal surface, and H be a non-trivial lattice plane of P . A *reflection twin* of P about H is a doubly periodic minimal surface Φ such that

- Φ is invariant under the action of $\text{Sym}(H)$ and under the reflection in H ;
- There is a sequence of Euclidean isometries $(T_k)_{k \in \mathbb{N}}$ such that $(T_k(\Phi))_{k \in \mathbb{N}}$ converges to P in a half-space.

Note that we only control the asymptotic behavior of Φ , but not the behavior near the twin boundary. Hence a surface, even dramatically different from P near H , would be admitted as a reflection twin of P . This is open for future debates.

A reflection twin has a single symmetry plane H , hence not periodic in the normal direction of H . Machineries to deal with non-periodic minimal surfaces were proposed in [Morabito and Traizet, 2012]; see also [Traizet, 2013]. This could lead to rigorous treatment of reflection twin if combined with the techniques in [Traizet, 2008]. The current paper presents numerical experiments, and the aperiodicity becomes inconvenient as computers do not really understand infinity. Therefore, we will work with *polysynthetic twins* with parallel reflection planes.

Definition 2. Let $P \subset \mathbb{R}^3$ be a triply periodic minimal surface, and H be a of non-trivial lattice plane of P . A *polysynthetic twin* of P (or a P *twin*) about H is a minimal surface Φ_n such that

- Φ_n is a triply periodic minimal surface of genus $2n + 1$;
- Φ_n is invariant under the action of $\text{Sym}(H)$;
- Φ_n is invariant under the reflection in H and in another lattice plane H' parallel to H ;
- the part of Φ_n between H and H' is “similar” to P .

Here the word “similar” is not well-defined in general. For rPD twins, the “similarity” will be reflected in the Weierstrass representation; see Definition 3. For Surface Evolver calculations, the program provides a operational definition of “similar”; see Sections 3.5 and 4.1.

A polysynthetic twin has infinitely many parallel reflection planes. The subscript n corresponds to the smallest separation between these twin boundaries. In the following, the word “polysynthetic” will be omitted unless otherwise stated.

3. THE rPD TWIN SURFACES

3.1. The rPD surfaces. The rPD-family is a 1-parameter family of TPMS with rhombohedral symmetries generalizing Schwarz’ D and P surfaces. A Weierstrass representation for the translational

unit of an rPD surface is given by [Fogden, 1993][Fogden and Hyde, 1999]

$$P_t: \omega \mapsto \operatorname{Re} \int^\omega (1 - z^2, i(1 + z^2), 2z)R(z) dz,$$

where $\omega \in \mathbb{C}$,

$$R(z) = [z(z^3 - t^3)(z^3 + t^{-3})]^{-1/2},$$

and $t > 0$ is the parameter. The Schwarz' D and P surfaces are restored with $t = \sqrt{1/2}$ and $t = \sqrt{2}$, respectively. The rPD-family is self-conjugate; the conjugate surface of P_t is $P_{1/t}$.

The rPD surfaces are known to [Schwarz, 1972] and rediscovered by [Schoen, 1970] and [Karcher, 1989]. They fall into Meeks' 5-dimensional family [Meeks, 1990]. In the Weierstrass representation of a Meeks' surface, the Gauss map represents the translational unit as a two-sheeted cover of \mathbb{S}^2 with four antipodal pairs (eight in total) of simple branch points. The branch points correspond to the flat points on the surface. For instance, after a stereographic projection onto the complex plane \mathbb{C} , the branch points of P_t are the roots of $R(z)^{-2}$.

The Weierstrass data reflects the symmetries of the rPD surfaces. More specifically, the surface has vertical symmetry planes (parallel to the z -axis). The group generated by these reflections is the Euclidean triangle group with parameters $(3, 3, 3)$. [Weyhaupt, 2006] proved that an embedded TPMS of genus 3 with these symmetries must be an rPD surface or an H surface.

We recommend the following way to visualize rPD surfaces. Consider two equiangular triangles that intersect the z -axis perpendicularly at their centers, whose projections on the xy plane differ by a rotation of $\pi/3$. Our building block, which we call *catenoid unit*, is the "catenoid" spanned the two triangles. The whole surface is obtained by order-2 rotations about the edges of the triangles. In the case of D and P surfaces, the z -axis is in the [111]-direction of the cubic lattice. If the projections of the triangles coincide on the xy plane, then the same construction yields an H surface. Catenoid units of H surfaces will appear on the twin boundaries of rPD twins.

The 1-parameter family is obtained by "stretching" the two triangles along the z -axis. Let $h(t)$ denote the height of the catenoid unit (vertical distance between the triangles) assuming unit inradii for the triangles, and $A(t)$ be the area of the catenoid assuming unit total area for two triangles. Using the formulae given in Appendix A of [Fogden and Hyde, 1999] (where the parameter r_0 correspond to our $1/t$), we plot h and A against t in Figure 2. The calculations are done in Sage [The Sage Developers, 2016].

The height h attains its maximum $h_{\max} = 1.529295 \dots$ at $t_0 = 0.494722 \dots$ and converges to 0 in both limits $t \rightarrow \infty$ and $t \rightarrow 0$. With a distance bigger than h_{\max} , the triangles span no catenoid; the only minimal surface is the relative interiors of the triangles. Any $h < h_{\max}$ corresponds to two different rPD surfaces; the one with bigger t has smaller area.

The area A attains its maximum $S_{\max} = 1.163261 \dots$ at $t = 0.494893 \dots$ and converges to 1 in the limit $t \rightarrow 0$, to $1/3$ in the limit $t \rightarrow \infty$. The area exceeds 1 as long as $t < t_1 = 0.877598 \dots$. Hence for t between t_0 and t_1 , the catenoid is only a local minimizer for the area functional; the relative interiors of the triangles has smaller area.

Other interesting points are: $t = \sqrt{1/2}$ for the D surface; $t = \sqrt{2}$ for the P surface; $t = 1$ is a self-conjugate surface; and $t = 1/t_0$ is the rGPD surface according to [Fogden and Hyde, 1999].

3.2. A Weierstrass representation of rPD twins. [Fujimori and Weber, 2009] developed an approach to construct surfaces with vertical symmetry planes. Instead of a cover of \mathbb{S}^2 , the Gauss map descends to the quotient torus $\mathbb{C}/\langle 1, \tau i \rangle$, where $\tau \in \mathbb{R}_+$ is an adjustable parameter. For example, the Weierstrass representation of an rPD surface is given by [Weyhaupt, 2006][Weyhaupt, 2008]

$$P_\tau: \omega \mapsto \operatorname{Re} \int^\omega \left(\frac{1}{2}(G_\tau^{-1} - G_\tau), \frac{i}{2}(G_\tau^{-1} + G_\tau), 1 \right) dz,$$

where the Gauss map

$$G_\tau(z) = \left(\rho \frac{\vartheta(z; \tau)}{\vartheta(z - 1/2 - \tau/2; \tau)} \right)^{2/3}$$

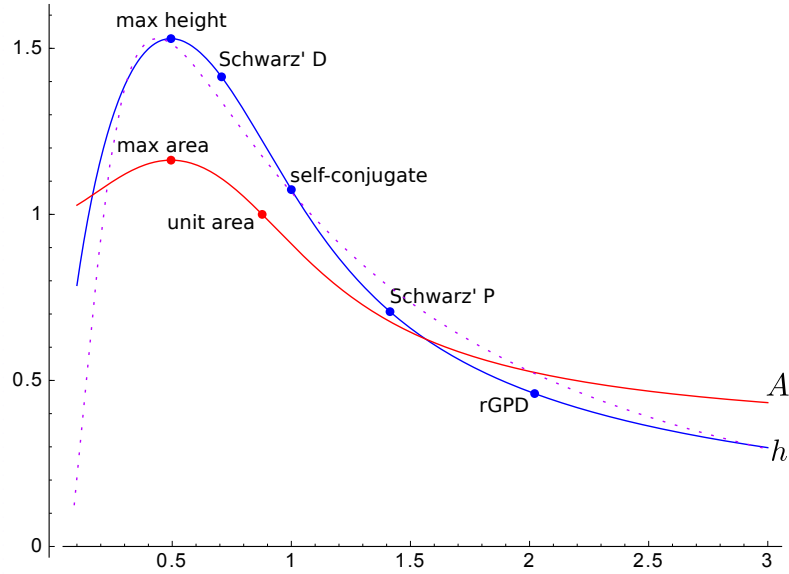


FIGURE 2. Plot of the height h (solid blue) of a catenoid unit assuming unit inradii for the bounding triangles, and the area A (solid red) assuming unit total area for the bounding triangles, against the parameter t on the horizontal axis. The dotted line is the reparameterization of h with the parameter τ in place of t on the horizontal axis.

is defined on the torus $\mathbb{C}/\langle 1, \tau i \rangle$. Here, ρ is the Lopez–Ros factor, and

$$\vartheta(z; \tau) = \sum_{k=-\infty}^{\infty} e^{-\pi(k+\frac{1}{2})^2\tau + 2\pi i(k+\frac{1}{2})(z-\frac{1}{2})}$$

is one of the Jacobi ϑ -functions; $\vartheta(z; \tau)$ has simple zeros at the lattice points spanned by 1 and τi . At the bottom of Figure 3, we show the zeros and poles of G_τ . They correspond to points of \mathbf{P}_τ with vertical normal vectors; these are exactly the flat points of \mathbf{P}_τ , and lie on the intersections of the vertical symmetry planes.

Note that τ is an equivalent but different parameter as t . For comparison, the height of the catenoid unit is plotted against τ by a dotted curve in Figure 2. The plot is generated by Sage [The Sage Developers, 2016], but the calculations are done using mpmath [Johansson et al., 2013]. The Schwarz’ P surface is restored with $\tau = 1.563401 \dots$ [Weyhaupt, 2006]. The relation between conjugate surfaces is similar: the conjugate surface of \mathbf{P}_τ is $\mathbf{P}_{1/\tau}$.

Apart from the vertical reflection planes, horizontal reflection planes are assumed in [Fujimori and Weber, 2009] in order to take advantage of the symmetry. Up to a translation, we may assume that one horizontal symmetry plane correspond to the imaginary axis of \mathbb{C} .

Following the argument in [Fujimori and Weber, 2009], we propose the following definition.

Definition 3. The rPD *twin surface* $\Phi_{\tau,n}$ is given by the Weierstrass representation

$$\Phi_{\tau,n}: \omega \mapsto \operatorname{Re} \int^\omega \left(\frac{1}{2}(G_{\tau,n}^{-1} - G_{\tau,n}), \frac{i}{2}(G_{\tau,n}^{-1} + G_{\tau,n}), 1 \right) dz,$$

where the Gauss map

$$G_{\tau,n}(z) = \rho \prod_{k \text{ odd}} \left(\frac{\vartheta((z - p_k)/n; \tau/n)}{\vartheta((z + p_k)/n; \tau/n)} \right)^{2/3} \prod_{k \text{ even}} \left(\frac{\vartheta((z - p_k - \tau/2)/n; \tau/n)}{\vartheta((z + p_k - \tau/2)/n; \tau/n)} \right)^{-2/3},$$

and $(p_k)_{1 \leq k \leq n}$ are real numbers such that $0 < p_1 < p_2 < \dots < p_n < n/2$ and $p_k + p_{n+1-k} = n/2$.

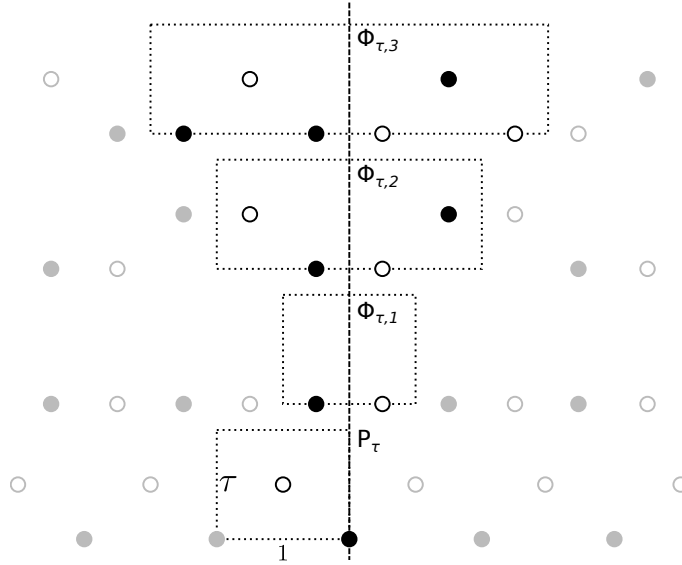


FIGURE 3. Zeros (filled circles) and poles (empty circles) of the Gauss maps G_τ and $G_{\tau,n}$, $n = 1, 2, 3$. The dotted rectangles indicate the tori on which the Gauss maps are defined.

Note that we scale the ϑ -function by $1/n$ so that, within the stripe $0 < \operatorname{Re}(z) < n/2$, the zeros and poles of $G_{\tau,n}$ are similarly arranged as for G_τ ; see Figure 3. The Lopez–Ros factor ρ is fixed to 1 so that $|G_{\tau,n}(z)| = 1$ for all $z \in i\mathbb{R}$; see Appendix A of [Weyhaupt, 2006].

3.3. Example and non-examples of small n . The fact that $\Phi_{\tau,n}$ satisfies the expected symmetries follows from [Fujimori and Weber, 2009]. But to prove their existence, we need to solve the period problem. In our case, the period problem for $\Phi_{\tau,n}$ asks to find p_k such that

$$\operatorname{Re} \int^{p_k} \left(\frac{1}{2}(G_{\tau,n}^{-1} - G_{\tau,n}), \frac{i}{2}(G_{\tau,n}^{-1} + G_{\tau,n}) \right) dz$$

are vertices of an equiangular triangle. In [Fujimori and Weber, 2009], the period problem is solved for small n 's, as an answer is immediate by symmetry. When $n = 1$ we have $p_1 = 1/4$; this is an H surface. When $n = 2$, we have $p_1 = 1/4$ and $p_2 = 3/4$; this is Karcher's T-WP surface.

For $n = 3$, the period problem is 1-dimensional. Examples of $\Phi_{t,3}$ are computed numerically. The Mathematica program for this purpose is kindly provided to us by Matthias Weber. The period problem asks to solve the following equations:

$$(1) \quad \begin{aligned} & \operatorname{Re} \int_0^{3/2+\tau/2} \frac{i}{2}(G_{\tau,3}^{-1} + G_{\tau,3}) dz = 0 \\ & \cos \frac{\pi}{6} \operatorname{Re} \int_{\tau/2}^{3/2} \frac{1}{2}(G_{\tau,3}^{-1} - G_{\tau,3}) dz + \sin \frac{\pi}{6} \operatorname{Re} \int_{\tau/2}^{3/2} \frac{i}{2}(G_{\tau,3}^{-1} + G_{\tau,3}) dz = 0 \end{aligned}$$

Under the symmetric assumptions $p_2 = 3/4$ and $p_1 + p_3 = 3/2$, the lhs of the equations are actually the same.

When we change τ to a very large value, Mathematica can not find any root. In Figure 4 we plot the lhs of (1) against $p_1/3$ for six values of τ , which clearly shows absence of solution for $\tau \geq 3$. In these plots we allow $p_1 > p_2 = 3/4$, in which case p_1 should be understood as p_3 ; the horizontal reflectional symmetry is then obvious. One observes that, as τ increases, p_1 and p_3 are pushed towards the center $p_2 = 3/4$, finally meet there and vanish. We calculate that $p_1 = p_2 = p_3 = 3/4$ when $\tau = 2.916517\dots$.

Observation 2. *There is a real number $T > 0$ such that the period problem for $\Phi_{t,3}$ has no solution for $t > T$.*

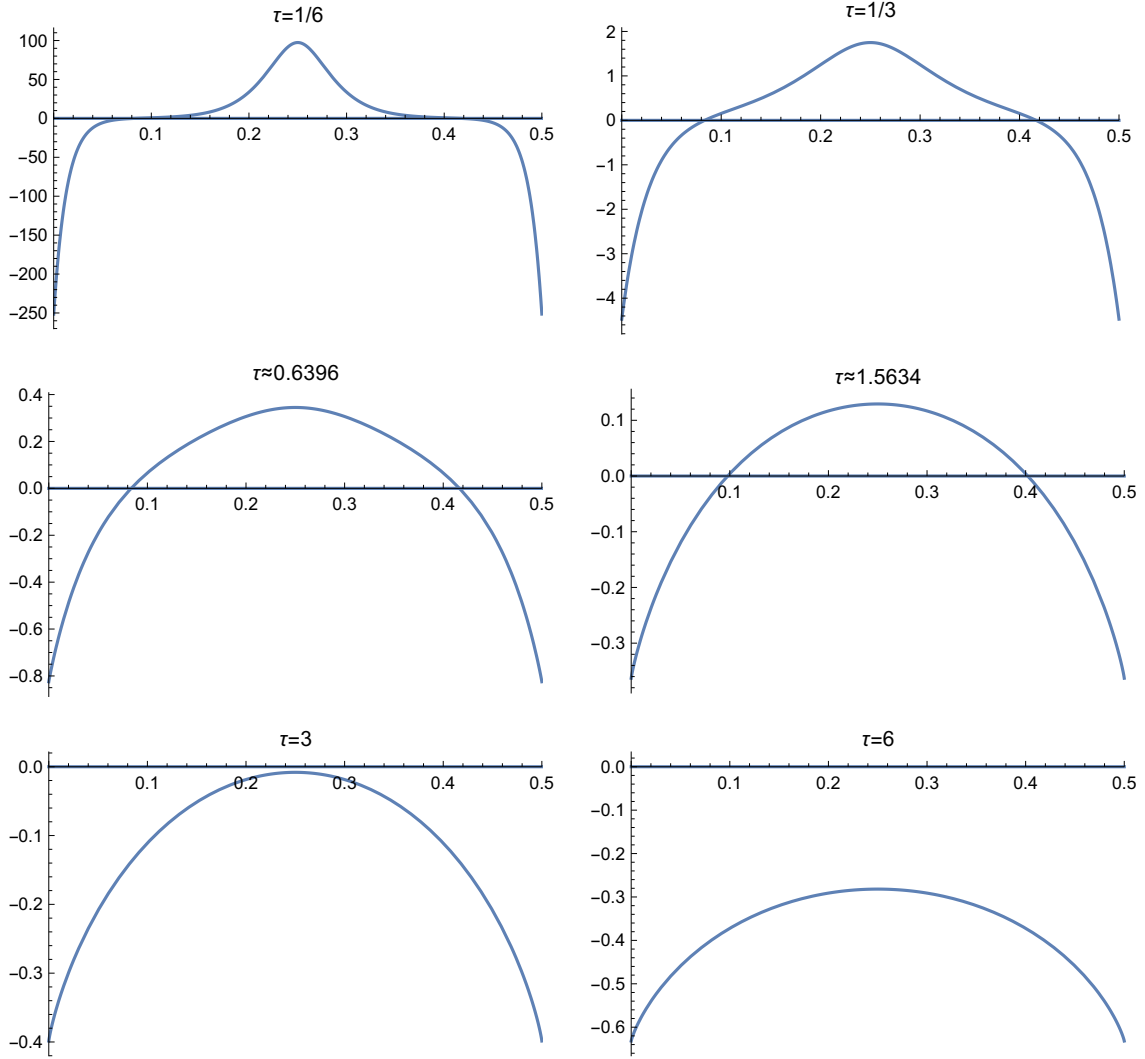


FIGURE 4. Plot of the lhs of (1) against $p_1/3$ for six different τ 's. In the middle row, the left is the twin of D surface, the right is the twin of P surface.

This observation is no surprise. The smaller the parameter t is, the closer the catenoid unit is to a standard catenoid. A standard catenoid has a natural horizontal symmetry plane, hence it is easier to twin P_t for small t . In the other limit $t \rightarrow \infty$, helicoids are forming. As the only properly embedded simply connected non-planar minimal surface in \mathbb{R}^3 [Meeks and Rosenberg, 2005], it is not possible to twin the standard helicoid. Hence twinning P_t with large t is expected to be difficult or impossible.

Another way to understand the situation is the following: On the one hand, when t is large, P_t is far from perpendicular to the horizontal planes. Hence to meet the free boundary condition on the twin boundaries, a larger perturbation would be needed. Under the perturbation, the flat points at height p_1 and p_3 is moving vertically towards p_2 . On the other hand, the flat points are already very close in the z direction, and there is little space for perturbation. These two factors together eliminates the possibility of twinning rPD surfaces with large t .

Numerical solution for larger n is challenging. But it is now reasonable to conjecture that

Conjecture 1. . *There is a monotonically decreasing function $T(n) > 0$, $n \geq 3$, such that the period problem for $\Phi_{t,n}$ has no solution for $t > T(n)$.*

3.4. Examples of small t . In the other end, for any n , the period problem is solved by [Traizet, 2008] for sufficiently small t . We now introduce his work.

Traizet was interested in TPMS with periods $(T_1, 0)$, $(T_2, 0)$ and (T_3, ε) which looks like infinitely many horizontal planes H_0, H_1, \dots with H_0 at $z = 0$ and H_N at $z = \varepsilon$, and adjacent planes are connected by small catenoid necks. As ε tends to 0, such a TPMS converges to a countably sheeted plane, and the catenoid necks converges to singular points arranged in the lattice spanned by T_1 and T_2 . We identify the plane to \mathbb{C} so that we can talk about positions and periods by complex numbers. Let m_k , $0 \leq k < N$, be the number of catenoid necks between H_k and H_{k+1} and $p_{k,i}$, $1 \leq i \leq m_k$, be the limit position of the i -th catenoid neck. The collection of $\{p_{k,i}\}$ together with the periods T_1, T_2, T_3 is called a *configuration*.

Given a configuration, [Traizet, 2008] defines the *force* on the i -th neck between H_k and H_{k+1} as follows:

$$(2) \quad \begin{aligned} F_{k,i} = & \sum_{j \neq i} \frac{2}{m_k^2} \zeta(p_{k,i} - p_{k,j}) \\ & - \sum_{k' = k \pm 1} \sum_j \frac{1}{m_k m_{k'}} \zeta(p_{k,i} - p_{k',j}) \\ & + \frac{1}{m_k} [(2x_k - x_{k-1} - x_{k+1})\eta_1 + (2y_k - y_{k-1} - y_{k+1})\eta_2], \end{aligned}$$

where

$$\zeta(z) = \frac{1}{z} + \sum_{0 \neq w \in \langle T_1, T_2 \rangle} \left(\frac{1}{z-w} + \frac{1}{w} + \frac{z}{w^2} \right)$$

is the Weierstrass ζ function; $\eta_i = 2\zeta(T_i/2)$, $i = 1, 2$; and the center of mass $\sum_j p_{k,j}/m_k = x_k T_1 + y_k T_2$. The configuration is said to be *balanced* if all the forces $F_{k,i}$ vanish, and *non-degenerate* if the differential of the map sending the positions $\{p_{k,i}\}$ to the forces $\{F_{k,i}\}$ has real co-rank 2. [Traizet, 2008] proved that, if the configuration is balanced and non-degenerate, then the TPMS described above exists and form a smooth family for sufficiently small ε .

The rPD surfaces with small t are examples of Traizet's surfaces; the configuration is given by

$$\begin{aligned} N = 2, \quad m_0 = m_1 = 1, \\ T_1 = 1, \quad T_2 = a = \exp(i\pi/3), \quad T_3 = 2(1+a)/3, \\ p_{0,1} = 0, \quad p_{1,1} = (1+a)/3. \end{aligned}$$

The balance and non-degeneracy has been proved in Section 4.3.3 of [Traizet, 2008]; see also Proposition 3 of the same paper.

The H surfaces are also examples; the only difference from the rPD surfaces is $T_3 = 0$. To verify Traizet's force balancing condition, consider the three integral of $\zeta'(z) = -\wp(z)$ along the directed segments shown in Figure 5. The Weierstrass elliptic function $\wp(z)$ is even and invariant under the action of $\langle 1, a \rangle$. The integrals sum up to 0 because of the symmetries. Therefore,

$$\left[\zeta\left(\frac{1+a}{3}\right) - \zeta\left(\frac{1}{2}\right) \right] + \left[\zeta\left(\frac{1+a}{3}\right) - \zeta\left(\frac{a}{2}\right) \right] + \left[\zeta\left(\frac{1+a}{3}\right) - \zeta\left(\frac{1+a}{2}\right) \right] = 0.$$

Since $\zeta(\frac{1}{2}) + \zeta(\frac{a}{2}) = \zeta(\frac{1+a}{2})$, we conclude that

$$-2\zeta\left(\frac{1+a}{3}\right) + \frac{4}{3}\zeta\left(\frac{1}{2}\right) + \frac{4}{3}\zeta\left(\frac{a}{2}\right) = 0.$$

Hence the configuration is balanced. The non-degeneracy is verified numerically.

At this point, crystallographers should notice the analogy of rPD and H family with the cubic and hexagonal closed packings. Within a period, there are three possible limit positions for the necks, namely $j(1+a)/3$ with $j = 0, 1, 2$. We then obtain an infinite sequence consisting of letters 0, 1 and 2. The rPD surfaces has a periodic sequence $\dots 012012012 \dots$. The sequences for rPD twins should be periodic and palindromic, like $\dots 010101010 \dots$ for the H surface, $\dots 012101210 \dots$ for the T-WP surface, etc.

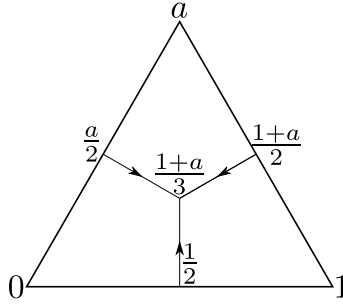


FIGURE 5. The integrals of $\zeta'(z) = -\varphi(z)$ along the three directed segments sum up to 0 because of the symmetry. This proves the force balancing condition for the H surfaces.

The formula (2) only involves adjacent layers. Up to symmetry, the only possible consecutive triples is 012 and 010, for which the force balancing condition has been verified in rPD and H surfaces. Hence the rPD twin configurations are all balanced and non-degenerate. Consequently, for any $n > 0$, there is a real number $\epsilon_n > 0$ such that the minimal twin surface $\Phi_{\tau,n}$ exists for $0 < \tau < \epsilon_n$. In fact, the argument works for any periodic sequence. For example, the sequence $\dots 0101201012 \dots$ also satisfy the force balancing condition.

Traizet's proof uses implicit function theorem. We do not know if the following conjecture holds.

Conjecture 2. *There is a positive number $\epsilon > 0$ such that the rPD-twin surface $\Phi_{\tau,n}$ exists for all $0 < \tau < \epsilon$ and $n > 0$.*

If this is the case, then for sufficiently small t , we could use a sequence of polysynthetic twins to approximate the reflection rPD twin. This seems plausible if one manages to combine the arguments in [Traizet, 2008] and [Morabito and Traizet, 2012]; see also [Traizet, 2013].

3.5. Numerical examples with Surface Evolver. Brakke's Surface Evolver [Brakke, 1992] is a software that simulates the physics of surfaces by minimizing energies. Surfaces are modeled by triangulations, and the energy is minimized by gradient descent method. Surface Evolver can handle various energies under various constraints.

In an usual application, the energy to minimize is the surface tension energy or the area functional. However, contrary to the intuition of many, TPMS do not result from area minimization. In the translational unit, a TPMS is actually a strict maximum of the area functional among its parallel surfaces [Große-Brauckmann, 2012]. A TPMS is indeed stable for the area functional if a volume constraint is imposed in the translational unit [Große-Brauckmann and Wohlgemuth, 1996]. But this is again false for any slightly larger piece [Ross, 1992]. Between two nearest twin boundaries, $\Phi_{t,n}$ correspond to a large piece of P_t , hence the area functional is not our option.

We will minimize instead the Willmore energy, or more precisely, the integral of the squared mean curvature; see [Hsu et al., 1992] for Surface Evolver experiments on this energy. Physically, the Willmore energy measures the deviation of the surface from the zero mean curvature, hence models the "bending" energy. The Willmore energy vanishes on minimal surfaces.

We construct the rPD twin surface $\Phi_{t,n}$ in Surface Evolver in four steps:

- (1) Prepare a catenoid unit.

Let $h = h(t)$ be the height function defined in Section 3.1. Consider four points

$$A(1, 0, 0), B(-1/2, \sqrt{3}/2, 0), C(-1, 0, h), D(1/2, \sqrt{3}/2, h).$$

The catenoid unit of P_t modulo reflectional symmetries is a minimal surface with fixed boundary conditions on the segments AB and CD , and free boundary conditions on the vertical planes $y \pm \sqrt{3}x = \sqrt{3}$. Reflections in these planes yield the whole catenoid unit. The boundary triangles has unit inradius, compatible with the discussions in Section 3.1. The unit is obtained in Surface Evolver by minimizing the area functional. As a consequence of this practice, we can only obtain rPD surfaces with parameter $t > t_0 = 0.494722 \dots$.

- (2) Generate a segment.

We generate a segment of P_t from the catenoid unit by order-2 rotations about the segment AB or CD . In Surface Evolver, this is done by listing the matrices, say \mathbf{a} and \mathbf{b} , of the two rotations in `VIEW.TRANSFORM_GENERATORS`. Assume an odd n , we set `transform_expr` to be a string $k(\mathbf{ba})$ if $n = 4k - 1$ or $k(\mathbf{ba})\mathbf{b}$ if $n = 4k + 1$. Then the Surface Evolver will display $n + 1$ catenoid unit. Finally, we use the `detorus` command to convert the displayed segment unit into a real surface.

- (3) Slice the segment.

In this step, we use Brakke's script `slicer.cmd` . It is included in the Evolver distribution, and also available on the website of Surface Evolver. It removes the part of the surface on one side of a given plane. We slice the segment in the previous step by two horizontal planes at offset 0.5 and separation n . The script also marks the vertices and edges newly created by the slice. This allows us to impose free boundary conditions by constraining the new vertices and edges on the slicing planes.

- (4) Evolve the surface.

We turn off the surface tension energy (`set facet tension 0`), and turn on the Willmore energy, which is the integral of squared mean curvature. Then we leave Evolver to minimize the energy. Apart from the command `g` that does one step of gradient descent, the command `hessian_seek` is particularly useful in this step to accelerate the calculation. If the Willmore energy decreases to practically 0, we obtain a minimal surface with free boundary condition on the boundary of a triangular prism. Reflections in the faces of the prism give the whole $\Phi_{t,n}$.

In Figure 6, we show the result of each step with $t = \sqrt{2}$ (Schwarz' P surface) and $n = 3$.

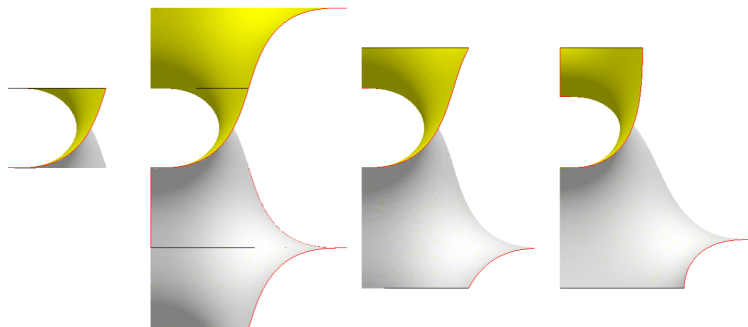


FIGURE 6. Result of each step with $t = \sqrt{2}$ and $n = 3$.

The program can be easily modified to change the parameters t and n . We perform calculations for parameters $t = t_0, \sqrt{1/2}$ (D), $1, \sqrt{2}$ (P), and $n = 1$ (H), $3, 5, 11, 21, 99$. When n is big, the last step will be very slow. We can increase the speed in the price of precision by reducing the number of faces in the catenoid unit. In Surface Evolver, the command `r` refines the surface by subdividing each triangle into four. When generating the catenoid unit, we refine five times for $n = 1, 3, 5$, four times for $n = 11, 21$ and three times for $n \geq 99$.

The calculation goes surprisingly smooth for small t and small n . For $t = t_0$ and $t = \sqrt{1/2}$ (D), the Willmore energy decreases quickly to the order of 10^{-26} or lower, even when $n = 99$. In view of the discussion in Section 3.3, it is reasonable to believe that the calculation would be even faster for smaller t . The results for $t = \sqrt{1/2}$ and $n = 3, 5, 11, 21$ are shown in Figure 7. The difference from the D surface is not visible with human eyes, hence we use CloudCompare [Girardeau-Montaut et al., 2016] to calculate the deviation from the D surface; the result for $n = 5$ is colored accordingly

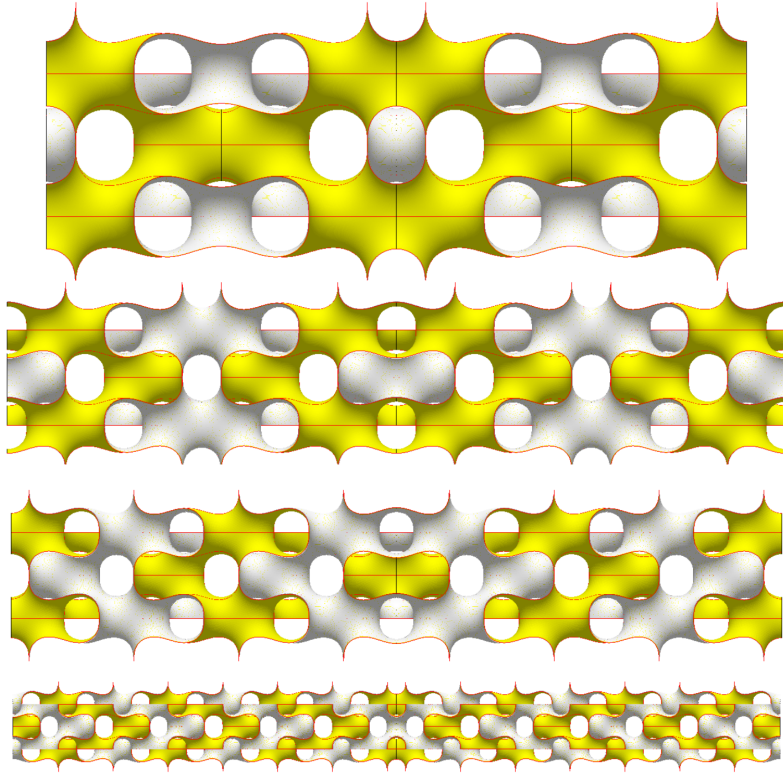


FIGURE 7. D twin surfaces ($t = \sqrt{1/2}$). From top to bottom, $n = 3, 5, 11, 21$. The twin boundary is clearly seen in the middle.

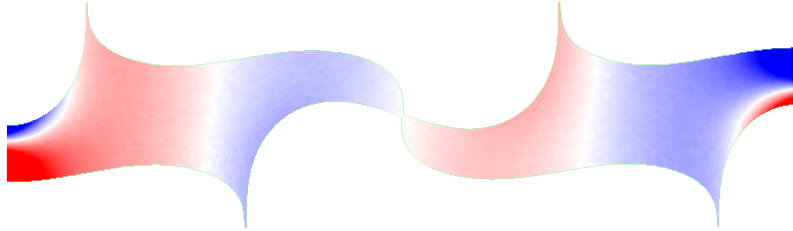


FIGURE 8. Deviation of the D twin with $n = 5$ from the D surface. Blue and red indicate perturbations in opposite directions; white indicates coincidence.

in Figure 8. We can see that the perturbation decays away from the twin boundaries, and the flat points are perturbed towards the middle. These pictures justify that the structure observed in [Han et al., 2011] is indeed a minimal D twin.

Observation 3. *The rPD twin surfaces $\Phi_{t,n}$ exist for a large set of parameters.*

In fact, if we obtain a minimal surface, the calculation roughly solves the period problem. More specifically, the vertices transformed from A or C when we generate the segment are the flat points, corresponding to the poles and zeros of the Gauss map $G_{\tau,n}$. After normalization, the heights of these points give the sequence $(p_k)_{1 \leq k \leq n}$. For example, the $\Phi_{\sqrt{1/2},3}$ (D twin) generated by Surface Evolver has twin boundaries at $z = \pm 3\sqrt{2}/2$, and the surface intersects the lateral edges of the prism at $z \approx 0$ and $z \approx \pm 1.41240$. By a scaling and a translation, we may place the boundaries at $z = 0$ and $z = 3/2$, and obtain $p_1 \approx 0.25064$, $p_2 \approx 0.75$ and $p_3 \approx 1.24936$. Compared to the solution given by the Mathematica program used for [Fujimori and Weber, 2009], these values are accurate until the fifth digit after the decimal point. However, the precision is not guaranteed as t

increases. The $\Phi_{\sqrt{2},3}$ (P twin) shown in Figure 6 gives $p_1 \approx 0.303350$, $p_2 \approx 0.75$ and $p_3 \approx 1.196651$, while Mathematica computes more precisely $p_1 = 0.293406\dots$, $p_2 = 0.75$ and $p_3 = 1.20659\dots$.

The Willmore energy also decreases to the order of 10^{-26} for $t = 1$ with $n \leq 21$, and for $t = \sqrt{2}$ with $n \leq 3$. However, for $t = 1$ and $n = 99$, the Surface Evolver only manages to reduce the Willmore energy to the order of 10^{-8} ; then the decrement becomes extremely slow. For $t = \sqrt{2}$ (P surface) and $n = 5$, the energy seems to stabilize at the order 10^{-4} . These calculations are therefore inconclusive.

Observation 4. *Surface Evolver does not converge to a minimal surface if t and n is too large.*

We then append more calculations for $t = \sqrt{1/2}$ to see if it eventually fails with sufficiently large n . It turns out that we are able to obtain a minimal surface with $n \leq 299$. Since the calculation is very time consuming for large n , we did not perform further computation. But the success with large D twins ensures that the inconclusive results for P twins do not arise from numerical or system errors. Hence we conjecture that $\Phi_{\sqrt{2},5}$ does not exist.

4. G TWIN SURFACES

4.1. Numerical examples with Surface Evolver. Twinnings of the G surface are also observed in experiment. Taking the flat points as lattice points, the twin boundaries are $\{211\}$ planes at offset 0.

Our Surface Evolver program for rPD twinning can be taken as an operational definition for “twinning”: Take a TPMS and impose free boundary condition on two parallel planes. If Surface Evolver is able to reduce the Willmore energy to practically 0, then the result is a twin minimal surface.

We then follow a similar procedure to generate G twin surfaces in Surface Evolver.

- (1) Prepare the G surface in an orthorhombic cell.

Unlike the rPD surfaces, the G surface contains no straight line, and has no symmetry plane. A datafile of initial triangulation is prepared by Fujita using the `torus` model of Surface Evolver. The orthorhombic unit cell is generated by three vectors in the $[0\bar{1}1]$, $[\bar{1}11]$ and $[211]$ directions. For our convenience, we made a small modification to place the $[211]$ direction on the z -axis.

Since this unit cell is larger than the translational fundamental cell, it is not safe to minimize the area functional [Große-Brauckmann and Wohlgemuth, 1996]. Hence we prepare the G surface by minimizing the Willmore energy directly.

- (2) Generate a segment.

In the `torus` model, the command `y 3` duplicates the displayed surface along the z -axis ($[211]$ -direction). Repetition of the command for k times would generate 2^k copies of the orthorhombic cell. We do not `detorus` the surface since we need the double periodicity.

- (3) Slice the segment.

Brakke’s script does not work well in the `torus` model, hence we write our own script to slice the segment by two horizontal planes ((211) planes) at offset 0, and impose free boundary conditions on the slicing planes.

- (4) Evolve the surface.

The program can be easily modified to adjust the separation n between the slicing planes (twin boundaries). We perform calculation for $n = 1, 2, 5, 10, 23$. In all these cases, we are able to obtain a minimal surface by reducing the Willmore energy to the order of 10^{-26} . We did not try larger separations. The results are shown in Figure 9. The G twin with $n = 1$ turns out to be an orthorhombic deformation of the D surface (an oD surface); this will be explained later. In Figure 10, the result for $n = 5$ is colored according to the deviation from the G surface.

Observation 5. *The G twin surfaces exist for a large set of parameters.*

4.2. A new insight into the G surface. The Gyroid surface is probably the most beautiful TPMS, but has the reputation of being difficult to visualize. For Surface Evolver, a datafile written by Große-Brauckmann back in 1995 is still widely used to generate the G surface. It decomposes

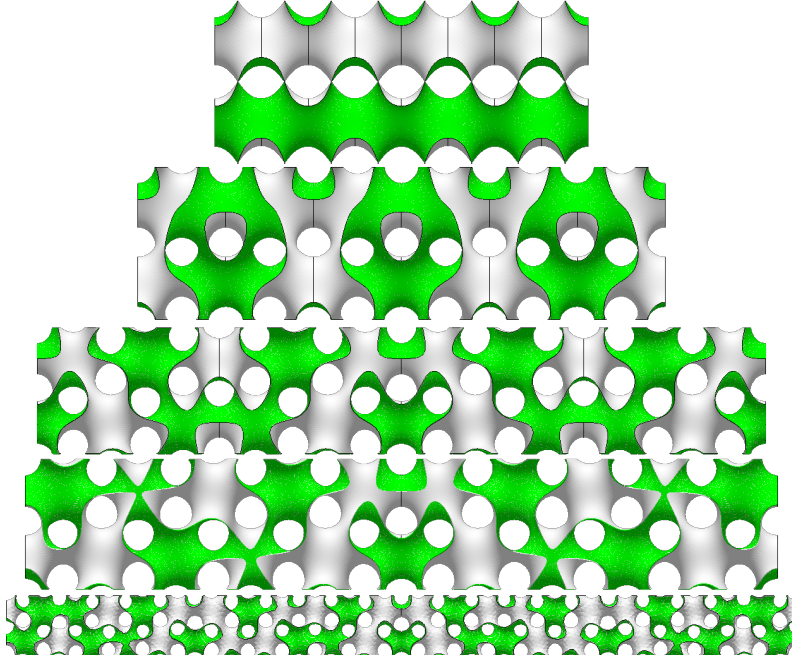


FIGURE 9. G twin surfaces. From top to bottom, $n = 1, 2, 5, 10, 23$. The twin boundary is clearly seen in the middle.

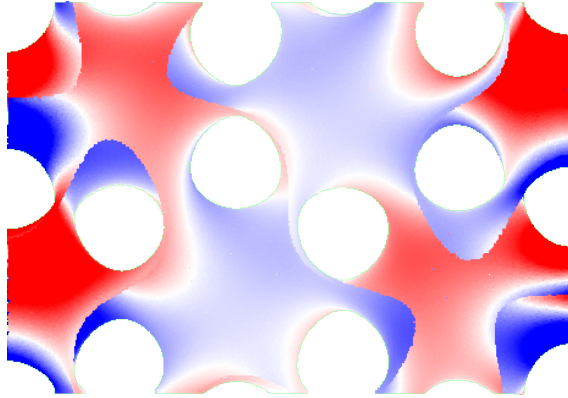


FIGURE 10. Deviation of the G twin with $n = 5$ from the G surface. Blue and red indicate perturbations in opposite directions; white indicates coincidence.

the cubic unit cell of the G surface into hexagons and rectangles, which is difficult to rewrite from scratch.

The (211) G twins reveal an interesting structure of the G surface which, to the knowledge of the author, was not mentioned before. In the upper half of Figure 11 is a gyroid sliced by $(0\bar{1}1)$ planes at offset 0.5. We observe necks arranged in a 2-D lattice. The lattice is spanned by vectors $T_1[\bar{1}11]$ and $T_2[111]$, and the difference between adjacent layers is $T_1/2$ or $T_2/2$ in an alternating manner. In the lower half of the same figure, we show the slices of the G twin with $n = 10$. We see clearly twinings of the 2-D lattice, and the twin boundary is parallel to T_1 .

This observation leads to a new way to construct the G surface in Surface Evolver. The initial triangulation in torus model is shown in the upper left corner of Figure 12. The monoclinic unit cell is spanned by $(\pm\sqrt{2}, 1, 0)$ and $(0, 0, 2\sqrt{2})$; this cell has the same volume as the cubic cell. We prepare four horizontal planes at $z = j\sqrt{1/2}$, $j = 0, 1, 2, 3$. Each plane is a 2-torus decomposed into four rhombi, labeled as in the figure. A rhombic tube connects the rhombi j between plane

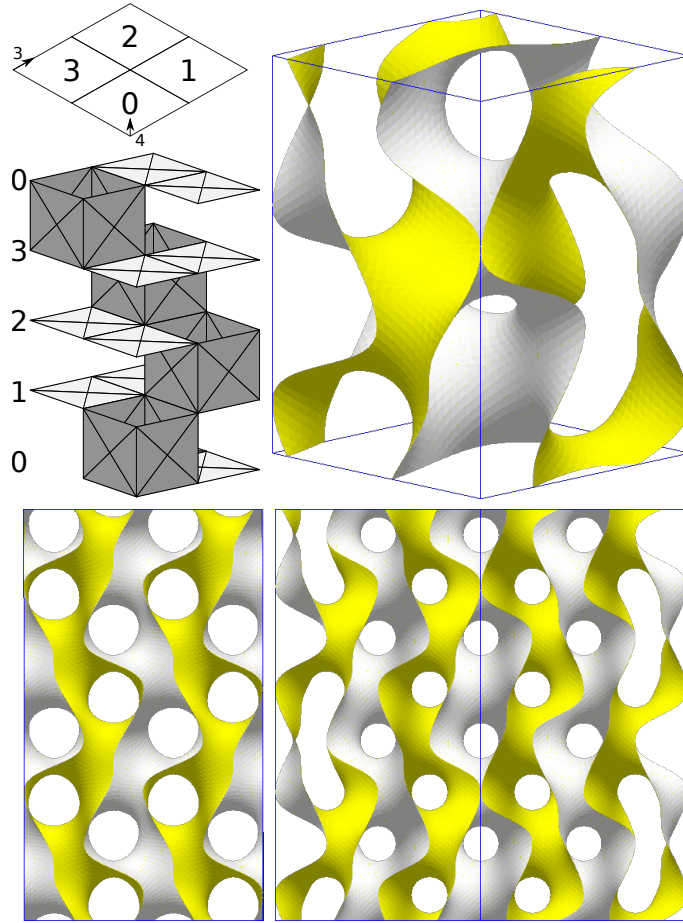


FIGURE 12. A new construction of the Gyroid in Surface Evolver. Upper left: the initial surface consists of four horizontal planes connected by tubes; see text. The small arrows indicates the direction of 3- and 4-fold axis. Upper right: Evolved result in a monoclinic unit cell. Lower left: Evolved result seen along the 3-fold axis. Lower right: Evolved result seen along the 4-fold axis.

Conjecture 3. *Within the alleged mG family, there is a continuous family of embedded deformations of the G surface that preserve the symmetry of the (011) planes and connects the G surface to the Traizet's surfaces.*

The mG family seems to contain, in particular, all the tetragonal deformations of the D surface (tD family [Fogden and Hyde, 1999]). To see this, notice the similarity between configuration (3) with $T_2 = iT_1$ and the diamond lattice. The (100) planes of the diamond lattice have the symmetry of square lattice, and adjacent (100) planes differ by a half-period in alternating directions.

The 2-D lattice for mG surfaces can be stretched along the diagonal ([100]) into a square of side length 2. We then repeat the program in the previous section with squares of side length 2 in place of the rhombi. The surface evolves into the D surface; see Figure 13. This is very surprising, yet completely reasonable. The other tD surfaces can be achieved by a vertical deformation. Based on this numerical evidence, we conjecture that

Conjecture 4. *The alleged mG family includes the tD family as special cases.*

The deformation we just speculated above provides a way to deform G into D in three steps: 1) vertically compress G near Traizet's limit; 2) horizontally deform the oblique 2-D lattice into a square lattice; and 3) vertically stretch the surface into D. If the horizontal deformation goes too

far, such that the rhombus becomes very elongated, then we would obtain a 4-fold “saddle tower”. All these behaviors are verified by our program; see Figure 13.

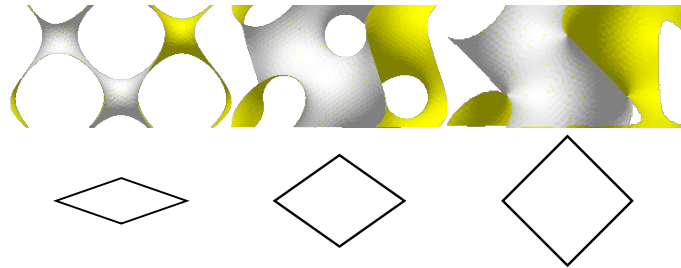


FIGURE 13. The diagonal of the rhombus (vertical in the figure) is a 4-fold axis of the G surface. By stretching the G surface (middle) in this direction, we obtain the D surface (right) and a 4-fold saddle tower (left). The surfaces shown in this figure are in the triclinic unit cell; the 4-fold axis is towards the readers. To be compared with tG surfaces in Figure 11 of [Fogden and Hyde, 1999].

Near Traizet’s catenoid limit, the mG surfaces can certainly be twinned about horizontal planes; the force balancing condition off the boundary is covered by (3), and the condition on the boundary is trivial. But in view of the G twin, we are more interested in twinning mG surfaces about vertical planes parallel to T_1 . We performed numerical calculations with $n = 1, 2, 3$. However, if we insist that the twin boundaries pass through the catenoid necks, the only balanced configurations turn out to be (3) with $T_1 = 1$, $T_2 = bi$ or $T_2 = 1 + bi$, where $b = \sqrt{8/9}$. This is not exactly what we observed in the G twins; thus our understanding of G twins, and more generally mG twins, is still very limited. Note that the case $T_2 = bi$ is an orthorhombic deformation of the D surface (oD) as we have observed, which should not be a surprise any more in view of previous discussions on the D surface.

For a concrete example of calculation, the configuration for $n = 1$ is (up to scaling)

$$(4) \quad \begin{aligned} N &= 4, & m_k &= 1 \quad (k = 0 \dots 3), \\ p_{0,1} &= 0, & p_{1,1} &= 1/2, \\ p_{2,1} &= x + 1/2 + bi/2, & p_{3,1} &= x + bi/2, \\ T_1 &= 1, & T_2 &= bi, & T_3 &= 0. \end{aligned}$$

The only solutions for $F_{0,1} = 0$ are $x = 0$ and $x = 1/2$.

REFERENCES

- [Brakke, 1992] Brakke, K. A. (1992). The surface evolver. *Experiment. Math.*, 1(2):141–165.
- [Fogden, 1993] Fogden, A. (1993). Parametrization of triply periodic minimal surfaces. III. General algorithm and specific examples for the irregular class. *Acta Cryst. Sect. A*, 49(3):409–421.
- [Fogden and Hyde, 1999] Fogden, A. and Hyde, S. T. (1999). Continuous transformations of cubic minimal surfaces. *The European Physical Journal B-Condensed Matter and Complex Systems*, 7(1):91–104.
- [Fujimori and Weber, 2009] Fujimori, S. and Weber, M. (2009). Triply periodic minimal surfaces bounded by vertical symmetry planes. *Manuscripta Math.*, 129(1):29–53.
- [Girardeau-Montaut et al., 2016] Girardeau-Montaut, D. et al. (2016). CloudCompare (Version 2.8.beta). Retrieved from <http://www.cloudcompare.org/>.
- [Große-Brauckmann, 2012] Große-Brauckmann, K. (2012). Triply periodic minimal and constant mean curvature surfaces. *Interface Focus*, 2:582–588.
- [Große-Brauckmann and Wohlgemuth, 1996] Große-Brauckmann, K. and Wohlgemuth, M. (1996). The gyroid is embedded and has constant mean curvature companions. *Calc. Var. Partial Differential Equations*, 4(6):499–523.
- [Han et al., 2011] Han, L., Xiong, P., Bai, J., and Che, S. (2011). Spontaneous formation and characterization of silica mesoporous crystal spheres with reverse multiply twinned polyhedral hollows. *Journal of the American Chemical Society*, 133(16):6106–6109.
- [Hsu et al., 1992] Hsu, L., Kusner, R., and Sullivan, J. (1992). Minimizing the squared mean curvature integral for surfaces in space forms. *Experiment. Math.*, 1(3):191–207.

- [Hyde et al., 1996] Hyde, S., Blum, Z., Landh, T., Lidin, S., Ninham, B., Andersson, S., and Larsson, K. (1996). *The Language of Shape*. Elsevier.
- [Johansson et al., 2013] Johansson, F. et al. (2013). *mpmath: a Python library for arbitrary-precision floating-point arithmetic (version 0.18)*. <http://mpmath.org/>.
- [Karcher, 1989] Karcher, H. (1989). The triply periodic minimal surfaces of Alan Schoen and their constant mean curvature companions. *Manuscripta Math.*, 64(3):291–357.
- [Meeks, 1990] Meeks, III, W. H. (1990). The theory of triply periodic minimal surfaces. *Indiana Univ. Math. J.*, 39(3):877–936.
- [Meeks and Rosenberg, 2005] Meeks, III, W. H. and Rosenberg, H. (2005). The uniqueness of the helicoid. *Ann. of Math. (2)*, 161(2):727–758.
- [Morabito and Traizet, 2012] Morabito, F. and Traizet, M. (2012). Non-periodic Riemann examples with handles. *Adv. Math.*, 229(1):26–53.
- [Ross, 1992] Ross, M. (1992). Schwarz' P and D surfaces are stable. *Differential Geom. Appl.*, 2(2):179–195.
- [Schoen, 1970] Schoen, A. H. (1970). Infinite periodic minimal surfaces without self-intersections.
- [Schwarz, 1972] Schwarz, H. A. (1972). *Gesammelte mathematische Abhandlungen. Band I, II*. Chelsea Publishing Co., Bronx, N.Y. Nachdruck in einem Band der Auflage von 1890.
- [The Sage Developers, 2016] The Sage Developers (2016). *SageMath, the Sage Mathematics Software System (Version 7.3)*. <http://www.sagemath.org>.
- [Traizet, 2008] Traizet, M. (2008). On the genus of triply periodic minimal surfaces. *J. Differential Geom.*, 79(2):243–275.
- [Traizet, 2013] Traizet, M. (2013). Opening infinitely many nodes. *J. Reine Angew. Math.*, 684:165–186.
- [Vignolini et al., 2012] Vignolini, S., Yufa, N. A., Cunha, P. S., Guldin, S., Rushkin, I., Stefik, M., Hur, K., Wiesner, U., Baumberg, J. J., and Steiner, U. (2012). A 3d optical metamaterial made by self-assembly. *Advanced Materials*, 24(10):OP23–OP27.
- [Weyhaupt, 2006] Weyhaupt, A. G. (2006). *New families of embedded triply periodic minimal surfaces of genus three in euclidean space*. ProQuest LLC, Ann Arbor, MI. Thesis (Ph.D.)—Indiana University.
- [Weyhaupt, 2008] Weyhaupt, A. G. (2008). Deformations of the gyroid and Lidinoid minimal surfaces. *Pacific J. Math.*, 235(1):137–171.

FREIE UNIVERSITÄT BERLIN, INSTITUT FÜR MATHEMATIK, ARNIMALLEE 2, 14195 BERLIN, GERMANY
E-mail address: hao.chen.math@gmail.com